Pis'ma v ZhETF, vol. 100, iss. 10, pp. 766 – 773

Ultra-hard $AlMgB_{14}$ coatings fabricated by RF magnetron sputtering from a stoichiometric target

A. M. Grishin[+*×1)], *S. I. Khartsev*[*], *J. Böhlmark*[+], *M. Ahlgren*[+]

[+] *AB Sandvik Coromant, SE-126 80 Stockholm, Sweden*

[*] *KTH Royal Institute of Technology, SE-164 40 Stockholm-Kista, Sweden*

[×] *Petrozavodsk State University, 185910 Petrozavodsk, Russia*

Submitted 15 October 2014

For the first time hard aluminium magnesium boride films were fabricated by RF magnetron sputtering from a single stoichiometric ceramic $AlMgB_{14}$ target. Optimized processing conditions (substrate temperature, target sputtering power and target-to-substrate distance) enable fabrication of stoichiometric in-depth compositionally homogeneous films with the peak values of nanohardness 88 GPa and Young's modulus 517 GPa at the penetration depth of 26 nm and, respectively, 35 and 275 GPa at 200 nm depth in 2 μm thick film.

DOI: 10.7868/S0370274X14220160

1. Introduction. In 1970, V.I. Matkovich and J. Economy exploring in Carborundum Company different refractory B_{12} borides had extracted small $AlMgB_{14}$ crystals from a mixture of aluminum borides prepared by heating B and Al to 1000–1400 °C. Mg was present as an impurity in the boron used for the experiments. They determined crystals structure to be orthorhombic with the cell dimensions $a = 10.313$ Å, $b = 8.115$ Å, and $c = 5.848$ Å and described it as a three dimensional network formed from icosahedral B_{12} groups [1]. The next three decades works on $AlMgB_{14}$ were mainly dedicated to refinement its crystal structure, true stoichiometry $Al_{0.75}Mg_{0.78}B_{14}$ [2], thermoelectric, electronic and optical properties (see references in Ref. [3]). Renewed interest $AlMgB_{14}$ had attracted at first in 1993 and then in 2000 when Higashi et al. [4] and later Cook et al. from Iowa [3] reported exceptional hardness of these crystals as high as, respectively, 27.4–28.3 GPa [4] and 32–35 GPa [3]. The most important step in exploration of $AlMgB_{14}$ was implemented by the same Iowa group who fabricated superhard self-lubricating films by pulsed laser deposition (PLD) technique [5]. Obtained films' hardness ranged from 45 to 51 GPa became a real breakthrough as a response to the longstanding quest for hard coatings that can increase wear resistance of cutting tools. In 2007, Newtech Ceramics Inc. based on the Iowa's invention [6] started to commercialize aluminum magnesium boride and coined the name BAM for a rich family of materials that combine $AlMgB_{14}$ with another hard boride, carbide, and boron nitride ceramics. Despite a strong commercialization effort, the most reliable characteristics of BAM coatings were reported for PLD-made films [7, 8] while results on magnetron sputtering remain very limited.

Z. Wu et al. deposited BAM films using three separate Al, B, and Mg targets. The maximum hardness of 30.7 GPa, Young's modulus $\sim$194 GPa and boron content of 65 at. % (instead of theoretical 90.2 at. %) were achieved only by increasing the boron target sputtering power up to 11 W/cm^2 (Mg and Al targets sputtering power was, respectively, 0.34 and 0.45 W/cm^2, target-to-substrate distance was 11 cm) [9]. C. Yan et al. co-sputtered metallic AlMg (1:1) alloy and B targets. For boron target sputtering power of 2 W/cm^2 and target-to-substrate distance of 13 cm, most of the films were strongly Mg-deficient. The closest to the theoretical stoichiometry (Al:Mg = 1.7, instead of 0.96, and boron content of 79 at. %) was obtained when they decreased AlMg target sputtering power down to 0.2 W/cm^2. 500 nm thick film onto Si(100) substrate showed the hardness about 30 GPa at the indentation depth of 100 nm [10]. Q.U. Wenchao et al. used a B target powered at 9 W/cm^2 and a sectoral assembled metallic Al/Mg (5:3) target. Substrate temperature of 300 °C and Al/Mg target sputtering power of 0.45 W/cm^2 (target-to-substrate distance not shown) were found optimal to obtain the maximum hardness of 39 GPa and Young's modulus of 443 GPa [11]. W. Liu et al. made attempts to deposit BAM films using stoichiometric $AlMgB_{14}$ target. Although the target sput-

[1)] e-mail: grishin@kth.se

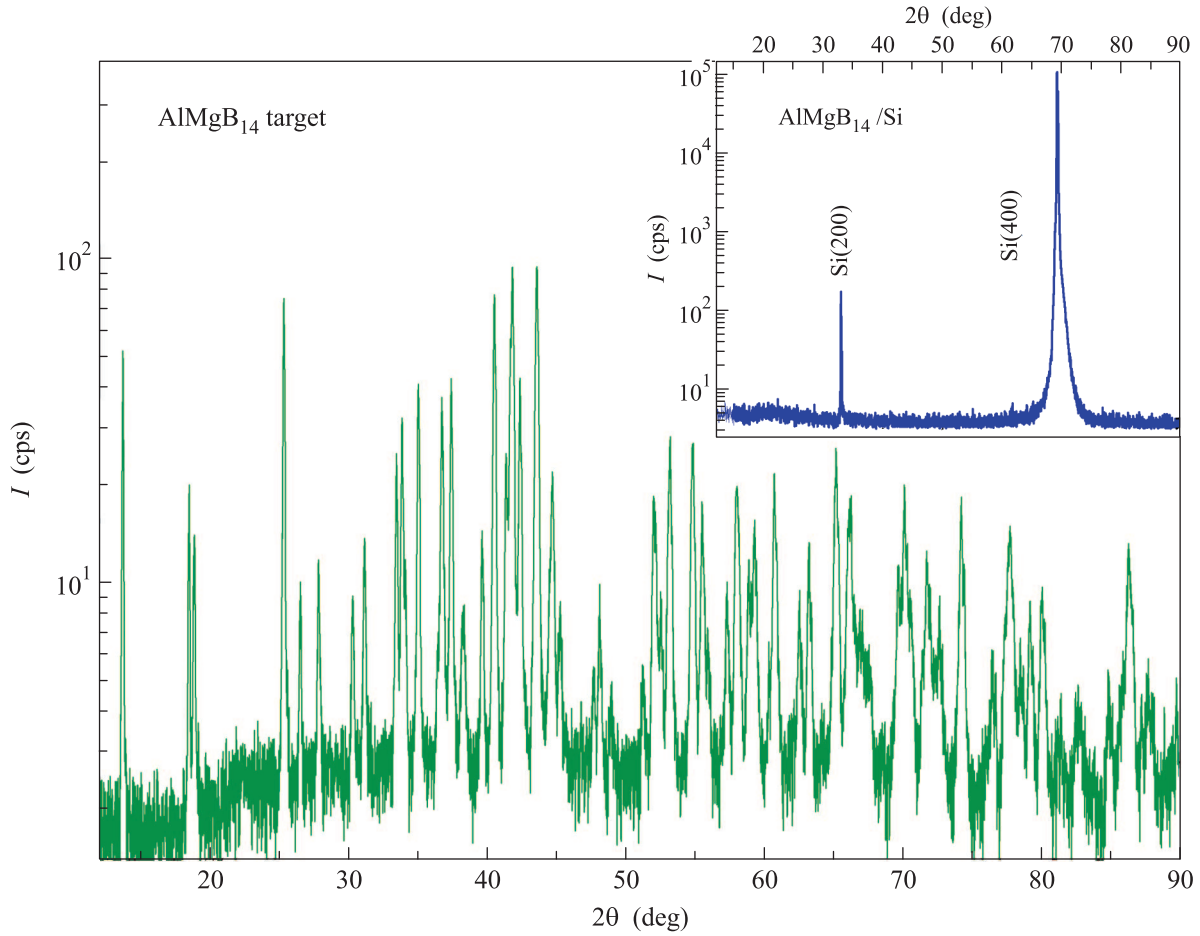

Fig. 1. XRD pattern of the surface of ceramic $AlMgB_{14}$ target subjected to RF sputtering. $\theta-2\theta$ scan recorded in Cu$K\alpha$ radiation is a superposition of two XRD spectra: orthorhombic $Al_{0.75}Mg_{0.78}B_{14}$ (from 2001 JCPDS-International Center for Diffraction Data, Card # 39-0459) and $MgAl_2O_4$ spinel phase (Card # 21-1152). Inset shows $\theta-2\theta$ scan of 0.4 μm thick BAM film deposited by RF magnetron sputtering onto Si(100) wafer at 550 °C

tering power was varied from 1 to 3.5 W/cm^2 (target-to-substrate distance was 8 cm) and substrate temperature varied from 25 to 600 °C, they could not obtain films with hard boride $AlMgB_{14}$ orthorhombic structure. At low temperatures films' surface was pocks and asperities rugged becoming smooth at 600 °C. Films were strongly in-depth inhomogeneous with an average Al, B, and Mg elemental content of 60, 30, and 10 at. %, correspondingly [12]. Fabrication of high quality BAM films by magnetron sputtering, which is well established technique in the cutting tool and component market, remains challenging.

Herein, we report the properties of aluminum magnesium boride films RF sputtered from a single ceramic $AlMgB_{14}$ target. High target sputtering power and a short target-to-substrate distance enable high-energy ballistic impact regime of adatoms' motion that results in BAM films' hardness ranged from 58 to 88 GPa.

2. Materials and methods. Batch of BAM films was deposited onto Si(100) wafers by sputtering of 1 inch stoichiometric $AlMgB_{14}$ target. The ultimate pressure in vacuum chamber was better than $3 \cdot 10^{-7}$ Torr, whereas films deposition was carried out at 7 mTorr of Ar-gas pressure. Substrate-to-target distance, RF power, and substrate temperature were varied to optimize film properties (in-depth uniformity, smooth surface, hardness) and to achieve the highest possible deposition rate. Finally, the distance of 25 mm between the 1 inch 50 W powered magnetron (target sputtering power is 10 W/cm^2) and substrate kept on the heater at 300 °C were found to be optimal to achieve the ultimate hardness of BAM films. At these conditions the deposition rate was found to be 0.44 nm/s.

Target that we used has a density of 1.45 g/cm^3 that is only 56 % of theoretical value. X-ray diffraction (XRD) $\theta-2\theta$ scan in Fig. 1 depicts a superposition

Table 1

Electron probe elemental analysis of films deposited at 250 and 550 °C

Element	Atomic number	Concentration of main elements, at. %				
		$T = 250$ °C			$T = 550$ °C	"Ideal"
		790 nm	1050 nm	1127 nm	1030 nm	$AlMgB_{14}$
Mg	12	4.05	3.77	3.69	2.25	5.02
Al	13	4.76	4.95	4.92	4.94	4.83
B	5	76.14	78.92	77.93	79.87	90.15
O	16	15.05	12.36	13.46	12.94	0
Sum		100				

of two XRD patterns: orthorhombic $Al_{0.75}Mg_{0.78}B_{14}$ (PDF Card # 39-0459) and $MgAl_2O_4$ spinel phase (PDF Card # 21-1152) [13].

3. Results and discussion. *3.1. Films structure and properties.* X-ray pattern of $AlMgB_{14}$ target in Fig. 1 abounds with multiple Bragg reflections. In contrast to the target, BAM films deposited onto Si wafer do not exhibit themselves with any XRD pattern even in a magnifying log-scale. θ–2θ scan of 0.4 μm thick BAM/Si film structure in inset to Fig. 1 contains only main Si(h00) wafer's peaks. All BAM films deposited at different temperatures varied from room temperature up to 550 °C were found to be X-ray amorphous.

Electron probe micro-analyzer (EPMA) used to check the stoichiometry of BAM coatings also confirmed amorphous character of deposited films. With the highest electron microscopy resolution, topographical images did not resolve any morphological (crystalline) features onto films' surface. Table 1 shows the results of elemental analysis of films fabricated at two different temperatures 250 and 550 °C. The biggest deficit of magnesium (the relative content was 2.25 instead of 5.02 at. %) and the biggest Mg:Al unbalance (the relative ratio was 0.46:1 instead of 1.04:1) were observed in the film deposited at 550 °C.

The highest Mg vapor pressure is liable to the re-sputtering of magnesium. Due to a slow deposition rate thus a long deposition time, it was observed even at 250 °C. Table 1 evidences that for three films with thicknesses 790, 1050, and 1127 nm Mg:Al ratio gradually decreases for thicker films as follows: 0.85:1, 0.76:1, and 0.75:1. More magnesium is re-sputtered as longer time film is exposed to a magnetron plasma etching. Surprisingly high oxygen concentration might be relied upon the presence of silicon oxide at the BAM/Si interface since the depth of oxygen X-ray emission at high electron energies exceeds films' thickness [14]. Noticeable decrease of oxygen content in thicker BAM@250 °C films (see Table 1) supports this assumption to some extent.

EPMA also revealed very in-plane uniform spatial distribution of Mg, Al, and B in BAM films compared to very inhomogeneous elemental contrast observed in $AlMgB_{14}$ target. Compositional image in the target consists of very contrastive domains: very bright corresponding to Al, darker from Mg, and the duskiest from B.

Optical transmission spectra in BAM films deposited onto Corning glass substrate are characteristic for semiconducting state (see Fig. 2). The absorption edge lies

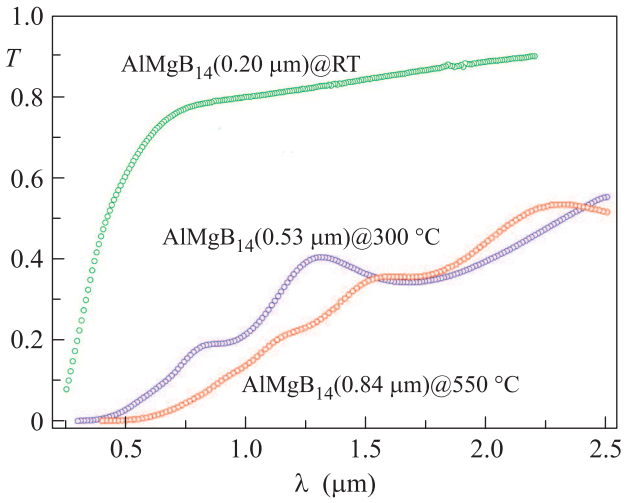

Fig. 2. Optical transmittance in BAM films grown onto the Corning 1737 glass substrate

around 275, 310, and 450 nm (bandgap is 4.5, 4, and 2.76 eV) and specific resistivity $\rho = (10–100)\,\mathrm{k\Omega \cdot cm}$, $1\,\Omega \cdot$ cm, and $8\,\Omega \cdot$ cm in films deposited, respectively, at RT, 300 °C and 550 °C. Films are very smooth. Their roughness measured with KLA-Tencor P-15 stylus profilometer does not exceed the roughness of the substrate (glass and Si wafers).

3.2. Nanohardness test. 20 different specimens deposited at various temperatures ranged from room temperature up to 550 °C were subjected to accurate nanohardness test measurements. Films hardness

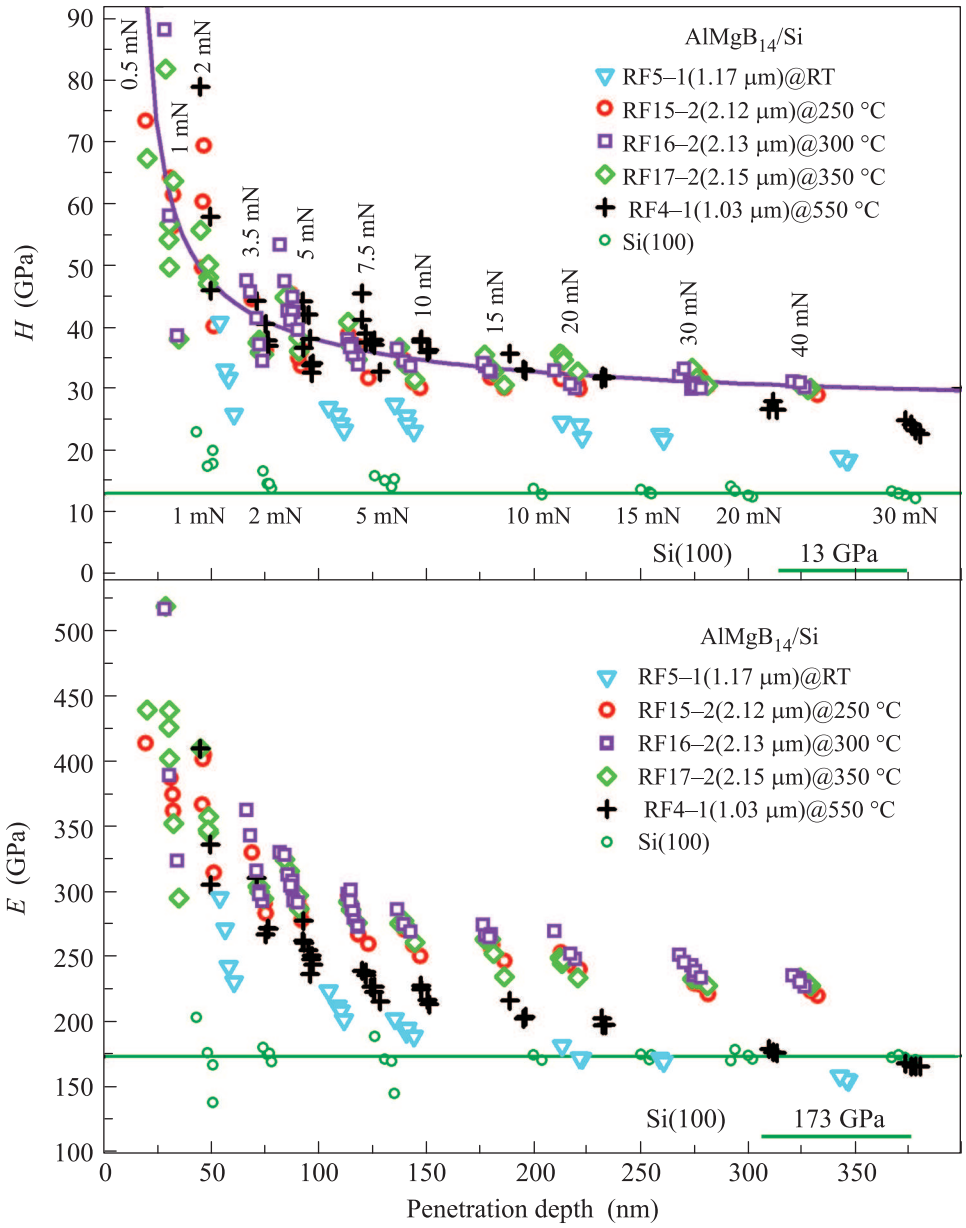

Fig. 3. Hardness H and elastic Young's modulus E vs. penetration depth measured in five different BAM films shown in Table 2. Numbers written above the group of symbols show the loading force in mN. Hardness of 13 GPa and Young's modulus of 173 GPa for single crystalline Si(100) wafer are shown for comparison

H [GPa] and elastic Young's modulus E [GPa] were characterized by $ST-Instrument$ nanohardness tester with Berkovich BO35 triangular diamond pyramid tip. The measurements were made with simple matrix 2×2 indentations repeated several times to exclude spurious indentations and collect reliable data sufficient for statistical averaging. New adjustment of the probe was performed every time for the next 2×2 indentations. Hardness and Young's modulus were measured at different loading forces ranged from 0.5 up to 40 mN. As commonly accepted, to obtain reliable nanohardness characteristics of thin films the penetration depth should not exceed 10–15 % of films' thickness. Therefore, although the deposition rate was very low and it took about 40 minutes to grow 1 μm thick film, we fabricated BAM films with a thickness exceeding 1 μm. This eliminates a role of Si substrate in the quantification of the nanohardness. Five the most representative specimens deposited at various temperatures and having different thicknesses were chosen for comparative analysis

Table 2

Characteristics of five specimens chosen for comparative nanoindentation tests

Specimen	Thickness, μm	Deposition temperature T, °C
RF5-1	1.17	RT
RF15-2	2.12	250
RF16-2	2.13	300
RF17-2	2.15	350
RF4-1	1.03	550

(see Table 2). The hardness and Young's modulus dependencies on penetration depth are presented in Fig. 3. The loading force in mN is shown with numbers written above the corresponding group of symbols.

Above mentioned limitation of the penetration depth restricts a peak value of a loading force since the penetration depth grows with a load as shown in Fig. 4. From

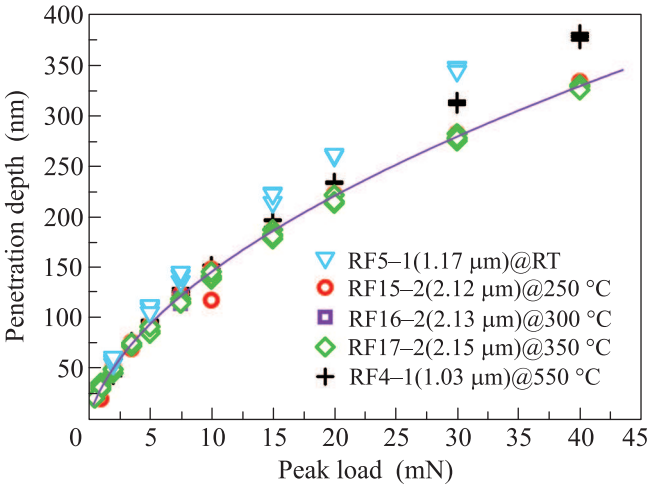

Fig. 4. Peak of a penetration depth as a function of the peak of a loading force applied to the indenter's tip. This dependence was obtained from the loading curves showing in the time domain how penetration depth grows when loading force increases

another side, measurements performed at too weak loading forces exhibit severe noise, appear to be much less reproducible and give big scattering of the data as clearly seen in Fig. 3. To find reliable range of the loading force that guaranties authentic data, we also performed the nanohardness test of blank 300 μm thick Si(100) wafer used for BAM films deposition. Results of these measurements are presented in Fig. 3 for comparison. As clearly seen, at loading force above 2 mN both hardness and Young's modulus of Si keep constant values about 13 and 173 GPa, respectively. These parameters are very close to the hardness $H = (10.5{-}13)$ GPa and elastic modulus $E = (130{-}185)$ GPa data reported in the literature for different directions in Si single crystal [15]. At weaker loads (1 mN) scattering of "bulk" Si data for Young's modulus E grows and hardness H increases indicating certain instrumental artifacts. Therefore, enormous growth of hardness and Young's modulus in BAM films at small penetration depths in Fig. 3 we cannot acknowledge with a complete confidence. It is worthy to note that similar tendency was observed by Iowa group (Fig. 3 in the Ref. [3]). Accounting abovementioned aspects, hereinafter we analyze results on hardness and Young's modulus that were obtained in BAM films at loading forces exceeding 2 mN. These experimental data are less scattered and show only weak dependence on the penetration depth which might be relied upon the in-depth inhomogeneity of films' properties. This issue we will discuss later in this paper.

3.3. In-depth films composition. Before we will conclude results on mechanical tests displayed in Figs. 3 and 4, it is worthy to comment the examination of elemental in-depth composition profiling in BAM films carried out by glow discharge optical emission spectroscopy (GDOES [16]). Besides the stoichiometry of BAM films this method gave us an insight on the nature of optimal deposition temperature. Fig. 5 display GDOES profiles recorded for four BAM films grown at different temperatures. Comparing these profiles we reached the following conclusions:

- RF5-1@RT is non-stoichiometric, almost 2 at. % B-depleted, Mg-to-Al overrich, Mg enriched at the film/substrate interface;
- RF3-1@550 °C is strongly non-stoichiometric, Mg:Al = 1:1 and are abundant in the film's interior, hence B becomes 3 at. % depleted at the film/substrate interface, Mg was re-sputtered and substituted by Al at the film surface;
- RF16-1@300 °C is stoichiometric, full-depth Mg:Al = 1:1 balanced, reasonable flat concentra-

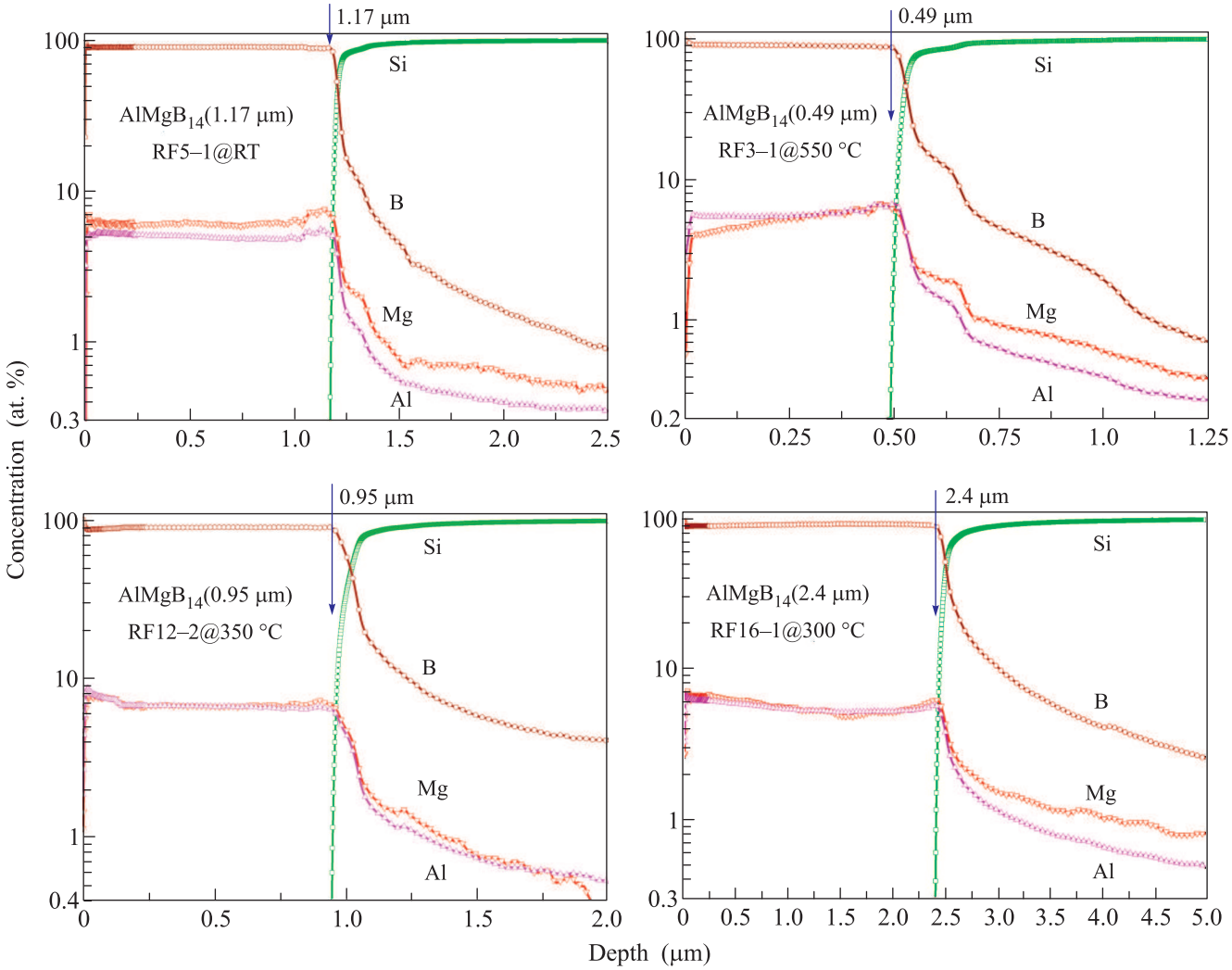

Fig. 5. Elemental concentration depth profiles in four $AlMgB_{14}$ films obtained using Glow Discharge Optical Emission Spectroscopy (GDOES). Vertical arrows show position of film/Si substrate interface defined by film's thickness measured by KLA-Tencor P-15 stylus profilometer

tion profiles though 1–2 at. % B-depleted at the film's surface and film/substrate interface;

- RF12-2@350 °C is non-stoichiometric, almost full-depth Mg:Al = 1:1 balanced, 3–4 at. % B-deficient in the film's interior and almost 7 at. % at the film's surface.

Non-etched remains of constituent film's elements at the periphery of ion-beam probe produce long tails in GDOES spectra. Generally, GDOES depth concentration profiles accord to EPMA composition data. They give the basis to explain processing temperature dependence of mechanical BAM films' properties we obtained from the indentation tests.

3.4. Mechanical characteristics. Three films RF15-2, RF16-2, and RF17-2 deposited within the "favourable" temperature range 250–350 °C show in Fig. 4 identical loading curves. All these data on maximum penetration depth achieved at different peak loads collapse into the single master curve

$$\text{Penetration Depth} = C \times (\text{Loading Force})^{1/2},$$

$$C = \sqrt{\frac{\pi(1-\nu^2)}{2E\,\mathrm{tg}(\vartheta/2)}} \qquad (1)$$

shown by a solid line with the constant $C = 53\,\mathrm{nm}/(\mathrm{m\,N})^{1/2}$. Eq. (1) is a standard expression for the contact between an elastic half-space of Young's modulus E and Poisson's ratio ν deformed by a rigid conical indentor with a cone angle ϑ (e.g. [17]). In contrast, two films RF4-1@550 °C and RF5-1@RT exhibit a lower stiffness: penetration depths achieved

at the same loading forces are bigger than those in "favourable" films. Such behaviour agrees with the reduction of Young's modulus E in RF4-1@550 °C and RF5-1@RT films that becomes especially apparent in Fig. 3 at loading forces above 10 mN. This effect we explain by the weakening of atomic bonds in non-stoichiometric aluminum magnesium boride.

The role of stoichiometry appears to be not so critical to govern films' hardness. Although RF5-1@RT film shows in Fig. 3 significantly lower hardness, in RF4-1@550 °C film H is comparable to the hardness of the films fabricated at "favourable" temperatures. Only at loading forces exceeding 20 mN, H rapidly decreases since the indentor "perceives" a soft Si substrate at greater penetration depths. Hardness is controlled by a plastic flow of defects, therefore a moderate hardness of RF4-1@550 °C sample we rely upon its sufficient compositional (though non-stoichiometric) homogeneity in the film's interior. However, at small penetration depths the nanohardness in Fig. 3 experiences big fluctuations reflecting strong Mg-to-Al unbalance that occurs at RF4-1@550 °C film surface and is manifested clearly by GDOES profile in Fig. 5.

Films RF15-2, RF16-2, and RF17-2 deposited at "favourable" temperatures show in Fig. 3 very regular much less scattered data both for hardness and Young's modulus. Within the examined 250–350 °C temperature range, film RF16-2@300°C demonstrates the best performance: the strongest Young's modulus, the highest hardness and the smallest variations even at the weakest loading forces ∼3 mN. Finally, we arrived to the conclusion that superior mechanical properties of magnetron sputtered aluminum magnesium boride films are governed by correct stoichiometry guarantying strong atomic bonds and high compositional in-depth homogeneity that can be achieved at the optimal deposition temperature of 300 °C.

This temperature optimal for magnetron sputtering appeared to be the same found by Iowa group in PLD process (see Fig. 3 and Ref. [3]). This coincidence seems to be natural since the performance of BAM films is critically related to their stoichiometry. At the same time, our films sputtered from stoichiometric target possess superior mechanical properties than PLD-made one. Besides the peak values $H = 88$ GPa and $E = 517$ GPa at small penetration depths against, respectively, 51 and 297 GPa [3], the hardness and Young's modulus in our RF16-2@300 °C sample are 35 against 28 GPa and 275 against 170 GPa, correspondingly, as compared at the penetration depth of 200 nm.

3.5. Elastic strain index. In Fig. 6 we drew the dependence of the nanohardness on the Young's modulus. This plot composed of a complete set of the same, as in

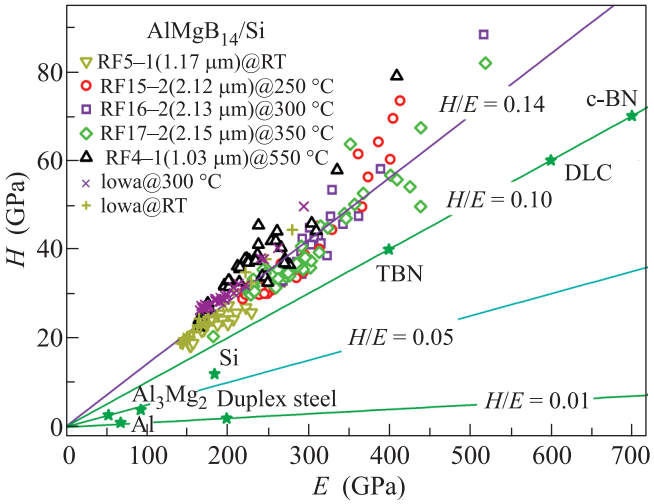

Fig. 6. Hardness vs. Young's modulus in examined five $AlMgB_{14}$ films compared to the H/E ratio in some engineering materials: cubic boron nitride (c-BN), diamond like carbon (DLC) and titanium boron nitride (TBN) films, bulk and Al_3Mg_2 coating [18] (latter has higher H and E values). Hardness and Young's modulus data in PLD-grown $AlMgB_{14}$ films reported by Iowa group (Fig. 3 in Ref. [3]) are marked up with × and + symbols. Solid lines present contours of constant ratios $H/E = 0.01$, 0.05, 0.1, and 0.14

Fig. 3, H and E data collected for all the indentations made at different loading forces in five BAM films sputtered at different temperatures. H vs. E data for films grown at "favourable" 250–350 °C temperatures form the most dense track along the straight line $H/E = 0.14$. A noticeable deviation occurs only at uncertainly high H and E obtained at too weak loading forces. The ratio of nanohardness H to Young's modulus E is known as the elastic strain index and considered as an indicative measure of the wear resistance of materials [19]. It is commonly assumed that a material with high H/E ratio like 0.1 possesses a better wear resistance than a material with a low ratio $H/E \sim 0.01$. For comparison, in Fig. 6 we also placed characteristics of several engineering materials (specified in Fig. 6 caption). Hardness vs. Young's modulus data reported in PLD-grown $AlMgB_{14}$ films [3] remarkably follow the same $H/E = 0.14$ ratio. They are marked up with × and + symbols in Fig. 6. This is an additional indication that besides extraordinary hardness $AlMgB_{14}$ coatings might be highly wear resistant.

4. Conclusion. Hardness H and Young's modulus E in $AlMgB_{14}$ films grown by RF magnetron sputtering were enhanced, respectively, by 25 and 62 % com-

pared to films made by pulsed laser deposition. Superior mechanical properties are attributed to films' high stoichiometry and compositional homogeneity. Elastic strain index H/E as high as 0.14 promises $AlMgB_{14}$ film coatings to possess also high wear resistance.

This research was funded by AB Sandvik Coromant.

1. V. I. Matkovich, J. Economy, Acta Crystallography B **26**, 616 (1970).
2. R. Schmechel and H. Werheit, J. Phys.: Cond. Matter **11**, 6803 (1999).
3. B. A. Cook, J. L. Harringa, T. L. Lewis, and A. M. Russel, Scripta Mater. **42**, 597 (2000).
4. I. Higashi, M. Kobayashi, S. Okada, K. Hamano, and T. Lundström, J. Crystal Growth **128**, 1113 (1993).
5. Y. Tian, A. F. Bastawros, C. C. H. Lo, A. P. Constant, A. M. Russell, and B. A. Cook, Appl. Phys. Lett. **83**, 2781 (2003).
6. B. A. Cook, Y. Tian, J. L. Harringa, A. P. Constant, A. M. Russell, and P. A. Molian, *U.S. patent* # 7.238.429 B2 (3 July 2007).
7. R. Cherukuri, M. Womack, P. Molian, A. Russell, and Y. Tian, Surf. Coat. Technology **155**, 112 (2002); Y. Tian, M. Womack, P. Molian, C. C. H. Lo, J. W. Anderegg, and A. M. Russell, Thin Sol. Films **418**, 129 (2002); Y. Tian, A. Constant, C. C. H. Lo, J. W. Anderegg, A. M. Russell, J. E. Snyder, and P. Molian, J. Vac. Sci. Technol. A **21**(4), 1055 (2003); Y. Tian, G. Li, J. Shinar, N. L. Wang, B. A. Cook, J. W. Anderegg, A. P. Constant, A. M. Russell, and J. E. Snyder, Appl. Phys. Lett. **85**, 1181 (2004); M. Stock, and P. Molian, J. Vac. Sci. Technol. A **22**(3), 670 (2004); J. C. Britson, *Pulsed laser deposition of $AlMgB_{14}$ thin films*, MSc. Thesis, Iowa State University (2008).
8. P. Blau, J. Qu, and C.B. Higdon, *Nanocoatings for high-efficiency industrial hydraulic and tooling systems*, Final Technical Report on Award # DE-FG36-06GO16054 (2010).
9. Z. Wu, Y. Bai, W. Qu, A. Wu, D. Zhang, J. Zhao, and X. Jiang, Vacuum **85**, 541 (2010).
10. C. Yan, Z. F. Zhou, Y. M. Chong, C. P. Liu, Z. T. Liu, K. Y. Li, I. Bello, O. Kutsay, J. A. Zapien, and W. J. Zhang, Thin Sol. Films **518**, 5372 (2010).
11. Q. U. Wenchao, W. U. Aimin, W. U. Zhanling, B. A. I. Yizhen, and J. Xin, Rare **31**, 164 (2012).
12. W. Liu, Q.-S. Meng, Y. Miao, F.-H. Chen, and L.-F. Hu, Adv. Mat. Res. **465**, 112 (2012).
13. JCPDS-International Center for Diffraction Data, Cards # 39-0459 ($Al_{0.75}Mg_{0.78}B_{14}$), # 21-1152 ($MgAl_2O_4$).
14. P. Willich and U. Wischmann, Mikrochim. Acta (Suppl.) **15**, 141 (1998).
15. B. Bhushan and X. Li, J. Mater. Res. **12**, 54 (1997); M. Ueda, C. M. Lepienski, E. C. Rangel, N. C. Cruz, and F. G. Dias, Surf. Coat. Technology **156**, 190 (2002); M. A. Hopcroft, W. D. Nix, and T. W. Kenny, J. Microelectromechanical Systems **19**, 229 (2011).
16. M. Wilke, G. Teichert, R. Gemma, A. Pundt, R. Kirchheim, H. Romanus, and P. Schaaf, Thin Sol. Films **520**, 1660 (2011).
17. S. Shimizu, T. Yanagimoto, and M. Sakai, J. Mater. Res. **14**, 4075 (1999).
18. S. Achanta, M. Feuerbacher, A. M. Grishin, X. Ye, and J.-P. Celis, Intermetallics **18**, 2096 (2010).
19. A. Leyland and A. Matthews, Wear **246**, 1 (2000).